

## Article

# Novel Porous Organic Polymer for High-Performance Pb(II) Adsorption from Water: Synthesis, Characterization, Kinetic, and Isotherm Studies

Saad Melhi <sup>1,\*</sup>, Eid H. Alosaimi <sup>1</sup>, Belal El-Gammal <sup>1</sup>, Wafa A. Alshahrani <sup>1</sup>, Yasser F. El-Aryan <sup>1</sup>, Hamdan A. Al-Shamiri <sup>2</sup> and Habib Elhouichet <sup>2</sup>

<sup>1</sup> Department of Chemistry, College of Science, University of Bisha, Bisha 61922, Saudi Arabia

<sup>2</sup> Department of Physics, College of Science, University of Bisha, Bisha 61922, Saudi Arabia

\* Correspondence: saadmelhi@ub.edu.sa

**Abstract:** The aim of the current study was to develop a novel triphenylaniline-based porous organic polymer (TPABPOP-1) by the Friedel–Crafts reaction for the efficient elimination of Pb(II) from an aqueous environment. XPS, FTIR, SEM, TGA, and <sup>13</sup>C CP/MAS NMR analyses were applied to characterize the synthesized TPABPOP-1 polymer. The BET surface area of the TPABPOP-1 polymer was found to be 1290 m<sup>2</sup>/g. FTIR and XPS techniques proved the uptake of Pb(II) was successfully adsorbed onto TPABPOP-1. Using batch methods, Pb(II) ion adsorption on the TPABPOP-1 was studied at different equilibrium times, pH values, initial Pb(II) concentration, adsorption mass, and temperature. The outcomes exhibited that the optimum parameters were t: 180 min, m: 0.02 g, pH: 5, T: 308 K, and [Pb(II)]: 200 mg/L. Nonlinear isotherms and kinetics models were investigated. The Langmuir isotherm model suggested that the uptake of Pb(II) was favorable on the homogeneous surface of TPABPOP-1. Adsorption kinetics showed that the PFO model was followed. Pb(II) removal mechanisms of TPABPOP-1 may include surface adsorption and electrostatic attraction. The uptake capacity for Pb(II) was identified to be 472.20 mg/g. Thermodynamic factors exhibited that the uptake of Pb(II) was endothermic and spontaneous in standard conditions. Finally, this study provides effective triphenylaniline-based porous organic polymers (TPABPOP-1) as a promising adsorbent with high uptake capacity.

**Keywords:** adsorption; porous organic polymers; Friedel–Crafts reaction; lead ion removal



**Citation:** Melhi, S.; Alosaimi, E.H.; El-Gammal, B.; Alshahrani, W.A.; El-Aryan, Y.F.; Al-Shamiri, H.A.; Elhouichet, H. Novel Porous Organic Polymer for High-Performance Pb(II) Adsorption from Water: Synthesis, Characterization, Kinetic, and Isotherm Studies. *Crystals* **2023**, *13*, 956. <https://doi.org/10.3390/cryst13060956>

Academic Editor: Sergio Brutti

Received: 11 May 2023

Revised: 9 June 2023

Accepted: 9 June 2023

Published: 15 June 2023



**Copyright:** © 2023 by the authors. Licensee MDPI, Basel, Switzerland. This article is an open access article distributed under the terms and conditions of the Creative Commons Attribution (CC BY) license (<https://creativecommons.org/licenses/by/4.0/>).

## 1. Introduction

As a result of intensive and increasing human activities, such as agriculture, mining, discharging batteries, and manufacturing industries, heavy metals contamination in water, which poses a serious threat to environmental health, has increased [1–4]. Lead (Pb(II)) is a toxic metal released from the effluent of batteries, paint, photographic materials, electronics, pigments, and automobile manufacturing units and into the environment [5]. Lead largely affects the central nervous system. In addition, it causes many disorders to human health such as vomiting, nausea, anemia, visual disturbances, loss of appetite, constipation, anemia, severe abdominal pain, and kidney damage [6–8]. The US EPA and WHO have defined a maximum permitted threshold for Pb(II) in drinking water to be 0.015 mg/L [9] and 0.01 mg/L [10], respectively, due to the health risks that Pb(II) poses to human health.

Many reliable approaches such as reverse osmosis, chemical precipitation, ion exchange, electrochemical methods, adsorption, and solvent extraction [11] have been developed for eliminating Pb(II) ions from industrial wastewaters. Among these methods, the adsorption method is simple, economically feasible, highly effective, and applicable for the elimination of different water contaminants. So far, various materials such as activated carbon [12], chitosan-saturated montmorillonite [13], ZnO nanoflowers [14],

CSt–ZnO nanocomposite [15], magnetite nanoparticles [16], EDTA–Zr(IV) iodate cation exchanger [17], thiol-modified activated carbon [18], and EG@CuFe<sub>2</sub>O<sub>4</sub> [19] have been developed for the elimination of Pb(II) ions from water contaminants. Porous adsorbent materials are for the most part considered effective adsorbents for toxic heavy metals and organic compounds [20].

Recently, hyper-crosslinking polymers (HCPs) characterize a novel class of low-cost porous polymer materials, comprising mostly microporous organic materials that can demonstrate a high surface area [21]. HCPs belong to the group of porous organic polymers (POPs), which are synthesized through the Friedel–Crafts alkylation reaction [22]. The permanent porous nature of HCPs is due to extensive crosslinking reactions, which prevent their chains from collapsing into a nonporous state and gives them high thermal stability [23]. HCPs with their high surface areas and lightweight nature have become a promising material for various applications, especially in environmental issues and clean energy, such as carbon dioxide capture, hydrogen storage, and toxic metal removal [24]. Hou et al. have developed a new facile strategy to synthesize hyper-crosslinked polymers through the Friedel–Crafts alkylation of aromatic cyclic hydrocarbons promoted by anhydrous AlCl<sub>3</sub> as a catalyst in the presence of dichloromethane as both an economical solvent and crosslinker. The obtained amorphous microporous networks with high surface area (978 to 1788 m<sup>2</sup>/g) exhibit good gas uptake capacities [25]. Additionally, this reaction only requires mild conditions and low-cost materials, presenting an economical and easier approach to the preparation of a set of porous organic polymers.

Different heavy metals were adsorbed by hyper-crosslinking polymers based on adsorbents such as sulfonated hyper-crosslinked polymers (SHCPs) [26], hydrophilic hyper-crosslinked polymers (HHCPs) [27], and thiol-rich 3D-porous hyper-crosslinked polymers [28]. El Hefnawy et al. prepared a new hyper-crosslinked nanometer-sized chelating resin (HCNSCR) for the elimination of Pb(II), Cd(II), and Zn(II) ions from solutions. They discovered that the HCNSCR's Zn(II), Pb(II), and Cd(II) ion adsorption capabilities were 0.9, 1.2, and 1.0 (mmol/ g), respectively [29].

Thus, the main objective of the current study was to develop a novel triphenylan-line-based porous organic polymer by a simple one-step Friedel–Craft reaction and evaluate its applicability for the elimination of lead ions from water. TPABPOP-1 consists of chelating amino (NH<sub>2</sub>) groups on its structure that act as adsorption sites. The TPABPOP-1 polymer' structures are shown in Figure 1. TPABPOP-1 was developed owing to its inherent characteristics of high surface area for efficient Pb(II) adsorption and easy preparation. The synthesized TPABPOP-1 was characterized by SEM, XPS, FTIR, <sup>13</sup>C CP/MAS NMR, and TGA analyses. Different parameters influencing the adsorption process were studied. The kinetics of adsorption, isotherms, and thermodynamics were achieved. Finally, the adsorption mechanism of Pb(II) using TPABPOP-1 polymer was clarified.

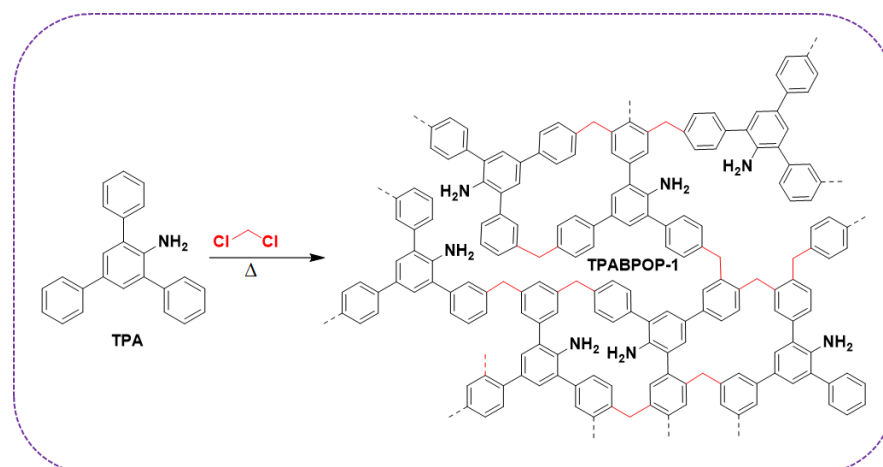


Figure 1. Synthesis of TPABPOP-1.

## 2. Materials and Methods

### 2.1. Materials

2,4,6-Triphenylaniline (97%), anhydrous dichloromethane (DCM), aluminum chloride ( $\text{AlCl}_3$ ), methanol,  $\text{Pb}(\text{NO}_3)_2$ , and tetrahydrofuran (THF) were purchased from Aldrich, and other chemical reagents (analytical grade) were used as received.

### 2.2. Instrumentation

The functional group determination of TPABPOP-1 before and after Pb(II) adsorption was studied using FTIR spectroscopy (Nicolet iS10 spectrometer, Thermo Scientific, Waltham, MA, USA) in the 400–4000  $\text{cm}^{-1}$  range. The surface area of TPABPOP-1 polymer was measured using a Micromeritics 3Flex analyzer, and the TPABPOP-1 sample was degassed at 120 °C for 12 h. Solid-state  $^{13}\text{C}$  (CP/MAS) NMR experiments were recorded on a Bruker Avance III 400 NMR spectrometer. The thermogravimetric analysis (TGA) of TPABPOP-1 was determined by a Pyris Diamond TGA in a nitrogen flow. Scanning electron microscopy (Hitachi Ltd., Tokyo, Japan) was applied to investigate the material's morphologies and elemental composition analysis of the TPABPOP-1 surface was conducted. An X-ray photoelectron spectrometer (XPS, Kratos, Manchester, UK) was used to determine the elemental composition of TPABPOP-1 and Pb(II)/TPABPOP-1. Inductively coupled plasma–optical emission spectroscopy (ICP–OES) was used to determine the residual number of Pb(II) ions in the aqueous medium.

### 2.3. Synthesis of TPABPOP-1

Triphenylaniline-based porous organic polymers (TPABPOP-1) were synthesized by the Friedel–Crafts reaction. Under a nitrogen atmosphere, 2,4,6-triphenylaniline (0.50 g, 1.56 mmol) was added to DCM (10 mL), then it was stirred for 10 min; next, anhydrous  $\text{AlCl}_3$  (5.00 g, 37.33 mmol) was added. After that, the mixture was reacted at RT for 1 h, followed by vigorous stirring for 8 h at 30 °C; for 12 h at 60 °C; and for 12 h at 80 °C. The mixture was cooled at ambient temperature, then the obtained precipitate was quenched using 15 mL HCl:  $\text{H}_2\text{O}$  (0.5:1(V/V)), then washed with water and methanol, respectively. Finally, the polymer (TPABPOP-1) was dried in a vacuum oven for 24 h at 65 °C (Figure 1).

### 2.4. Adsorption Experiments

The adsorption performance of TPABPOP-1 toward Pb(II) ions was examined by the batch method. The influence of initial concentrations (50–1000 mg/L), solution pH (2–7), contact time (20–500 min), and adsorption mass (0.005–0.025 g) were studied. Typically, a known amount of TPABPOP-1 adsorbent was transferred to an Erlenmeyer flask containing 30 mL of 100 mg/L Pb(II) solution. The initial pH of the sample was then controlled by 0.1 M  $\text{HNO}_3$ /NaOH solutions. The sample was then mechanically agitated for 180 min at 100 rpm, and the sample solution was then separated using filtering. The Pb(II) ion concentrations were determined by ICP–OES. The following Equations (1) and (2) were used to calculate the elimination effectiveness and equilibrium adsorption quantity of Pb(II) ions ( $q_e$ , mg/g), respectively, as follows:

$$\text{Adsorption efficiency (\%)} = \frac{C_0 - C_t}{C_0} \times 100 \quad (1)$$

$$q_e = (C_0 - C_t) \frac{V}{m} \quad (2)$$

where  $C_0$  (mg/L) and  $C_t$  (mg/L) represent the initial and final concentrations of Pb(II) at time  $t$ , respectively, in the solution. The weight of TPABPOP-1 is  $m$  (g), while the volume of the solution containing Pb(II) ions is  $V$  (L).

### 3. Results

#### 3.1. Characterization of TPABPOP-1

The FTIR spectra of TPABPOP-1 and TPABPOP-1/Pb(II) are displayed in Figure 2a. The broad peaks at  $3423\text{ cm}^{-1}$  were owing to the stretching vibration of  $\text{NH}_2$  [30]. A peak of around  $2973\text{ cm}^{-1}$  was described as a phenylic C–H bond. The two peaks at  $2926$  and  $2871\text{ cm}^{-1}$  were due to symmetrical and asymmetric aliphatic C–H stretching vibrations and  $\text{CH}_2$ , respectively, which implies that the crosslinking reactions are carried out efficiently [31]. The strong peak at  $1622\text{ cm}^{-1}$  and weak peak at  $1446\text{ cm}^{-1}$  were described as the N–H bending and C=C stretching of the aromatic ring group, respectively [32]. A peak at  $1378\text{ cm}^{-1}$  was ascribed to the  $-\text{NH}_2$  group [33]. The peaks in the range ( $1095$ – $1164\text{ cm}^{-1}$ ) were attributed to the stretching and bending of  $-\text{C}-\text{N}$  [34]. The decrease in intensity and apparent shift in transmittance from  $3423$ ,  $1622$ , and  $1164\text{ cm}^{-1}$  to  $3432$ ,  $1632$ , and  $1150\text{ cm}^{-1}$  confirmed that the  $\text{NH}_2$ , N–H bending, and C–N of the TPABPOP-1 adsorbent, respectively, were involved in the adsorption of Pb(II) by electrostatic interactions between the positive charge of Pb(II) and negative charge of the  $\text{NH}_2$  group on the TPABPOP-1 adsorbent [35].

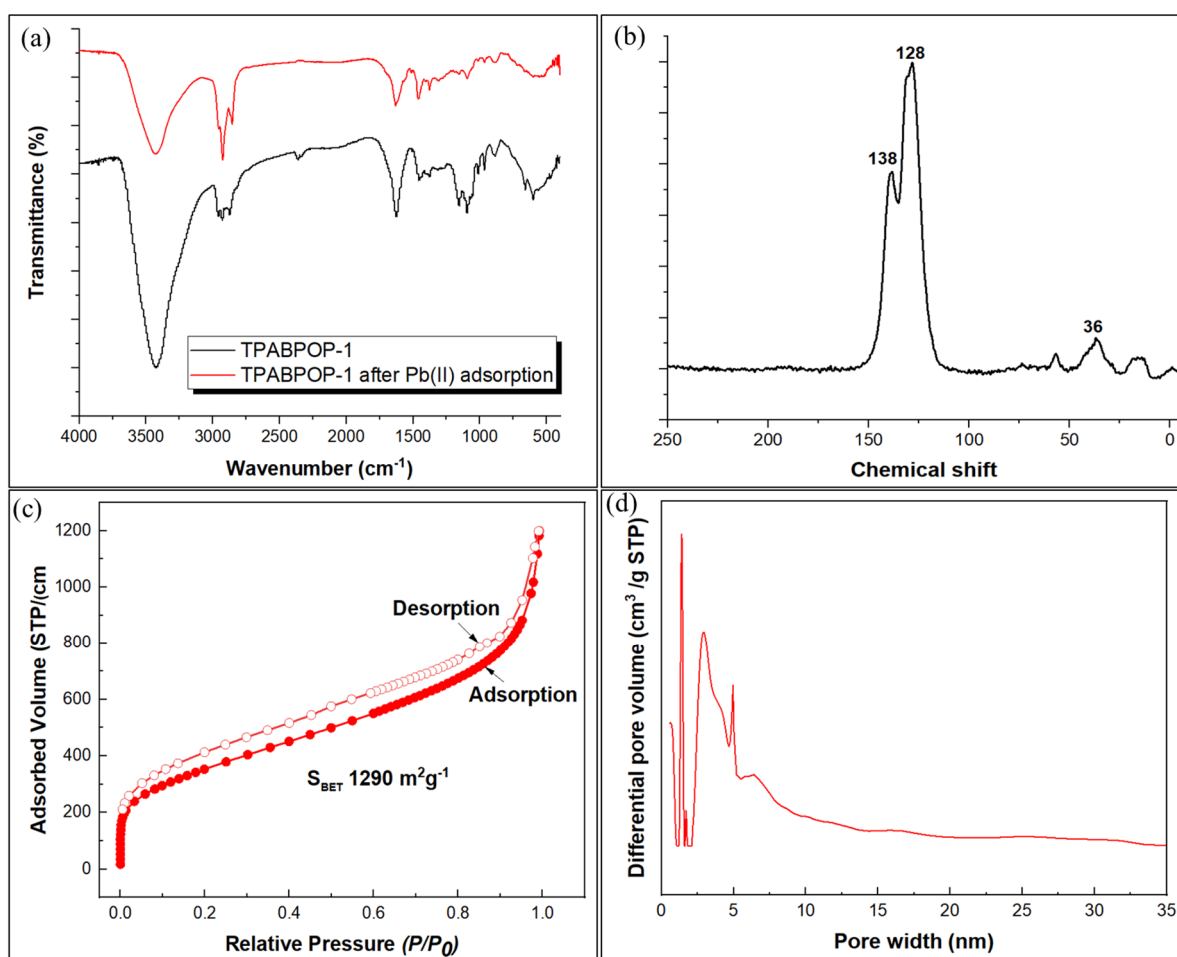


**Figure 2.** (a) FTIR spectra of TPABPOP-1 and TPABPOP-1/Pb(II), (b)  $^{13}\text{C}$  CP/MAS NMR, (c)  $\text{N}_2$  adsorption–desorption isotherm, and (d) pore size distribution of TPABPOP-1.

Figure 2b shows the  $^{13}\text{C}$  CP/MAS NMR spectra of TPABPOP-1. It was observed that the TPABPOP-1 displayed signals at chemical shifts ( $\delta$ ) of 118 and 138 ppm, attributed to substituted and unsubstituted aromatic carbons, respectively. A peak at 36 ppm was ascribed to the carbon of methylene, which was formed as a result of using dichloromethane (DCM) as a crosslinker and reaction solvent.

The N<sub>2</sub> adsorption–desorption isotherm of TPABPOP-1 as displayed in Figure 2c was classified as type IV, indicative of a microporous nature of TPABPOP-1. Furthermore, it was seen that the hysteresis of TPABPOP-1, a rapid increase at low pressure ( $p/p_0 < 0.01$ ), indicated the microporous nature of TPABPOP-1 [36]. TPABPOP-1 demonstrated a BET surface area of 1290 m<sup>2</sup>/g which is better than amino-linked porous organic polymers [36]. From the pore size distribution of TPABPOP-1, as shown in Figure 2d, we determine there are three peaks at 1.4, 2.9, and 5.3 nm indicating the microporous nature of TPABPOP-1.

The thermal stability of TPABPOP-1 is shown in Figure 3a. The initially small weight loss (4%) in the range of 30–150 °C was due to the release of entrapped solvent and water from the pores of TPABPOP-1 [37]. At 365 °C, the mass of the TPABPOP-1 decreased by 8% due to the initial breakdown of the TPABPOP-1's structure. Up to about 800 °C, the weight loss of the TPABPOP-1 declines by around 43%, which is ascribed to the increased degradation of TPABPOP-1. Hence, the TGA results show that the TPABPOP-1 has good thermal stability. Figure 3b,c exhibits the SEM image of surface morphologies of TPABPOP-1 with different magnification. It was observed that the surface of TPABPOP-1 has irregular blocks aggregated together [25].

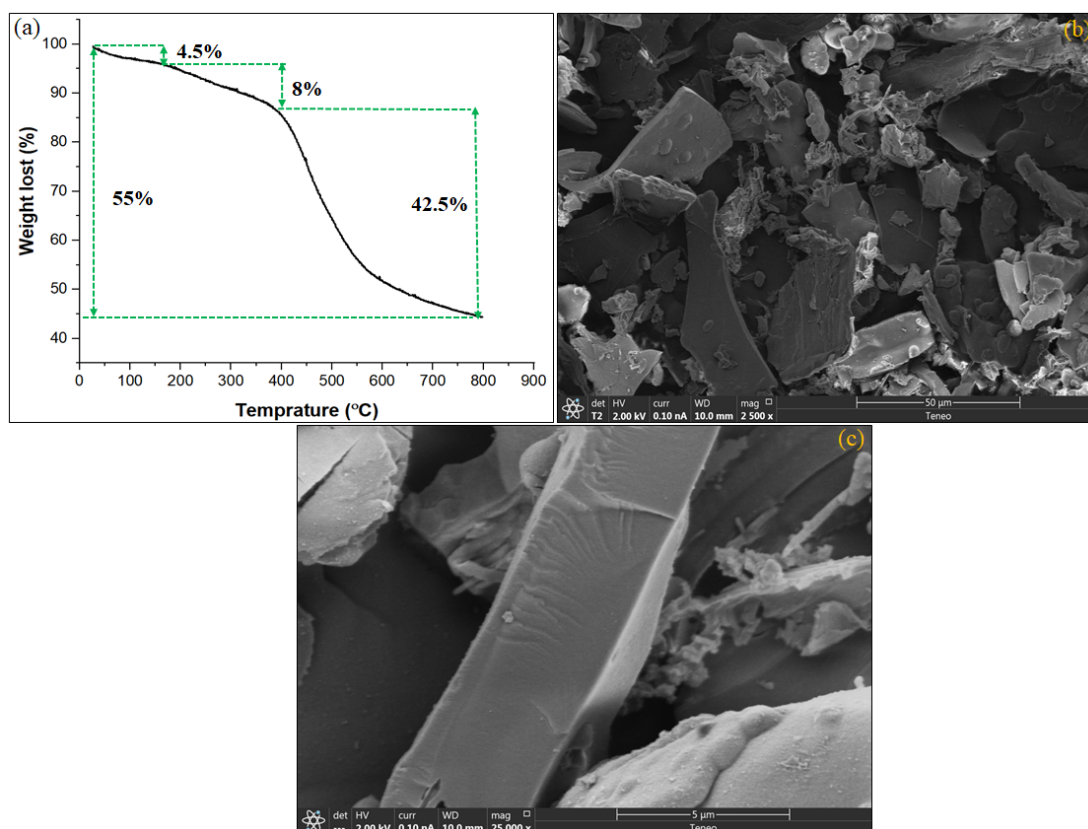


**Figure 3.** (a) TGA analysis and (b,c) SEM image of TPABPOP-1.

The XPS spectra of TPABPOP-1 and TPABPOP-1/Pb(II) are exhibited in Figure 4. It was seen that the XPS spectra of TPABPOP-1 exhibit two peaks at 284.86 and 399.52 eV attributed to carbon (C1s) and nitrogen (N1s), respectively [38]. Further, the O 1s peaks were observed as seen in Figure 4a, resulting from the physically adsorbed water or oxygen molecules which may be present in carbon-based materials. The same result was reported in a previous publication [39]. The deconvoluted N 1s spectrum shows one binding energy peak at 399.52 eV attributed to C–NH<sub>2</sub> as shown in Figure 4b. The high-resolution XPS spectrum for C 1s displays two peaks at 284.76 and 285.98 eV for C–C/C=C and C–N, respectively (Figure 4c). In the XPS spectra of Pb(II)/TPABPOP-1 after adsorption, two new

peaks appeared at 143.96 and 139.10 eV attributed to Pb 4f<sub>5/2</sub> and Pb 4f<sub>7/2</sub>, respectively [40], demonstrating that Pb(II) ions were effectively absorbed by TPABPOP-1 (Figure 4d).

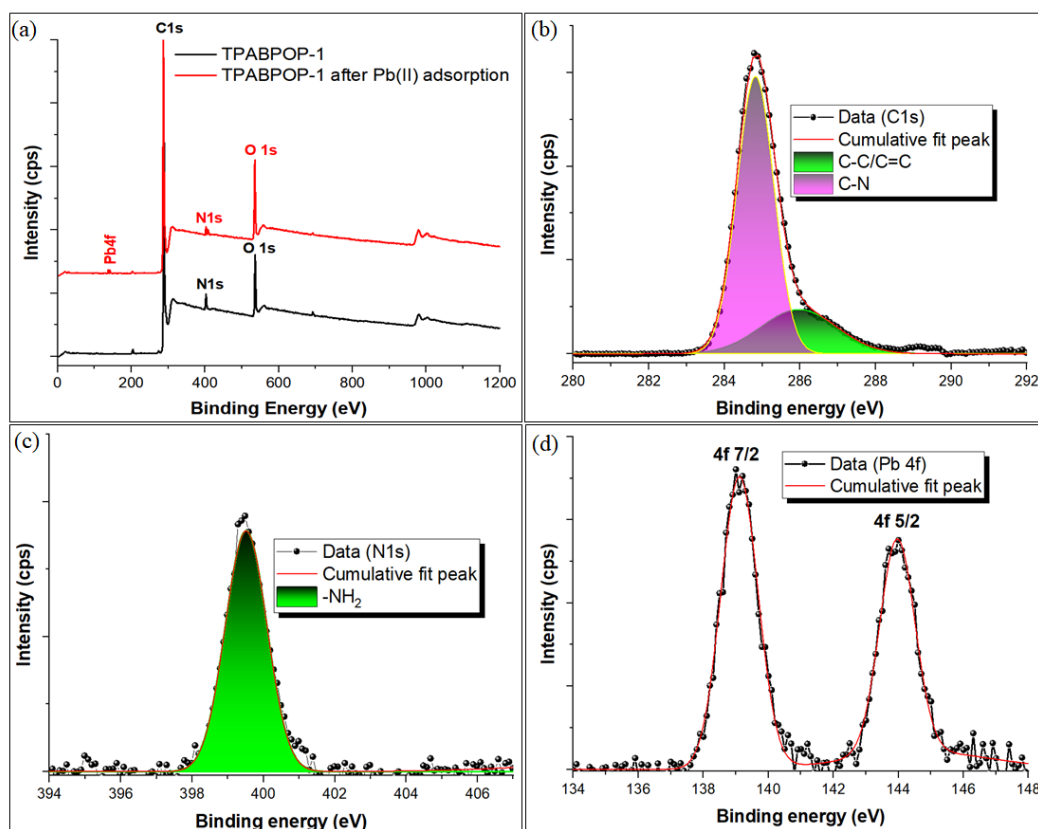


**Figure 4.** (a) XPS analysis for wide-scan spectrum of TPABPOP-1 and TPABPOP-1/Pb(II), (b) high-resolution C 1s, (c) N 1s, and (d) Pb 4f.

### 3.2. Adsorption Performance of TPABPOP-1

The influence of pH value on the uptake of Pb(II) by TPABPOP-1 was conducted by varying the pH from 2.0 to 7.0 under fixed conditions ([Pb]: 100 mg/L, t: 24 h., m: 0.02 g, and T: 298 K) as shown in Figure 5a. The equilibrium uptake capacity was enhanced from 16.5 to 145.5 mg/g with pH rising from 2 to 5. After pH reached a value of 5, the uptake capacity was slightly reduced to 139.5 mg/g, due to the change in the ionic state of the amino groups on the TPABPOP-1 surface. In a low-pH environment, the amino group on the TPABPOP-1 surface was protonated with H<sub>3</sub>O<sup>+</sup> became -NH<sub>3</sub><sup>+</sup>. Thus, electrostatic repulsion forces between -NH<sub>3</sub><sup>+</sup> groups and positively charged Pb(II) were created, which led to a reduction in the uptake capacity of TPABPOP-1. When the solution pH (2 ≤ pH ≤ 5) increased, the amino groups were deprotonated on the TPABPOP-1 surface and electrostatic attraction forces between positive Pb(II) and negative amino groups on the surface of TPABPOP-1 were created, which increased TPABPOP-1's ability to adsorb Pb(II) ions. The effect of pH on the Pb(II) speciation distribution was observed at pH > 7. According to the Pb(II) speciation diagram for Pb(II), which was reported in a previous publication [41], the main Pb(II) species are Pb<sub>3</sub>(OH)<sub>4</sub><sup>2+</sup>, Pb(OH)<sub>2</sub>, and Pb(OH)<sub>3</sub><sup>-</sup> at pH > 7. The uptake capacity of adsorbent toward Pb(II) ions was decreased at pH > 6 due to the Pb(II) ions being precipitated as Pb(OH)<sub>2</sub> [42]. Therefore, at pH > 7, adsorption studies were not performed because of the precipitation of Pb(II). Thus, a pH of 5 was chosen for subsequent Pb(II) adsorption experiments. Similar observations were reported for Pb(II) adsorption on PANINSA@Ni<sub>0</sub>CNs [43] and Fe<sub>3</sub>O<sub>4</sub>@MCM-41-N-oVan [44].

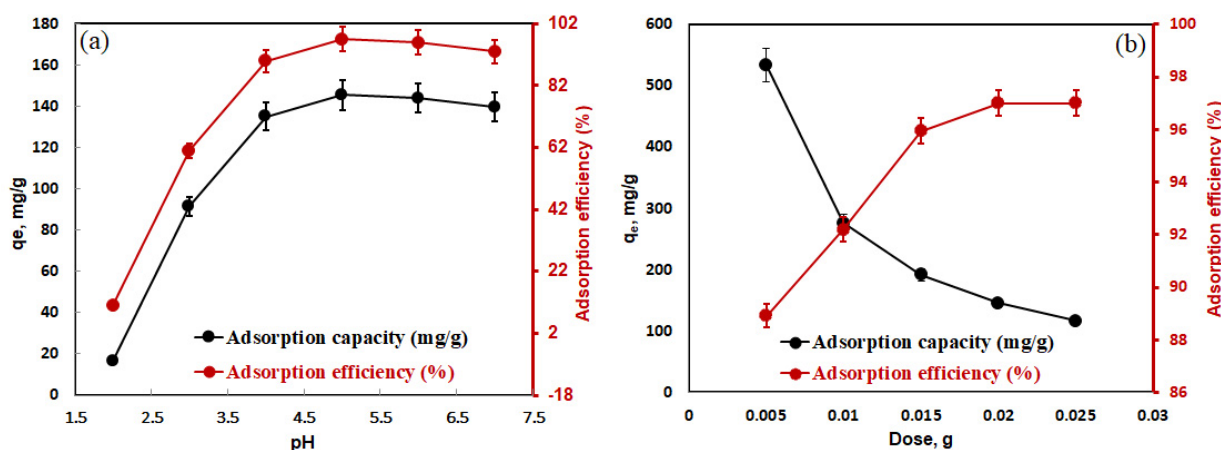
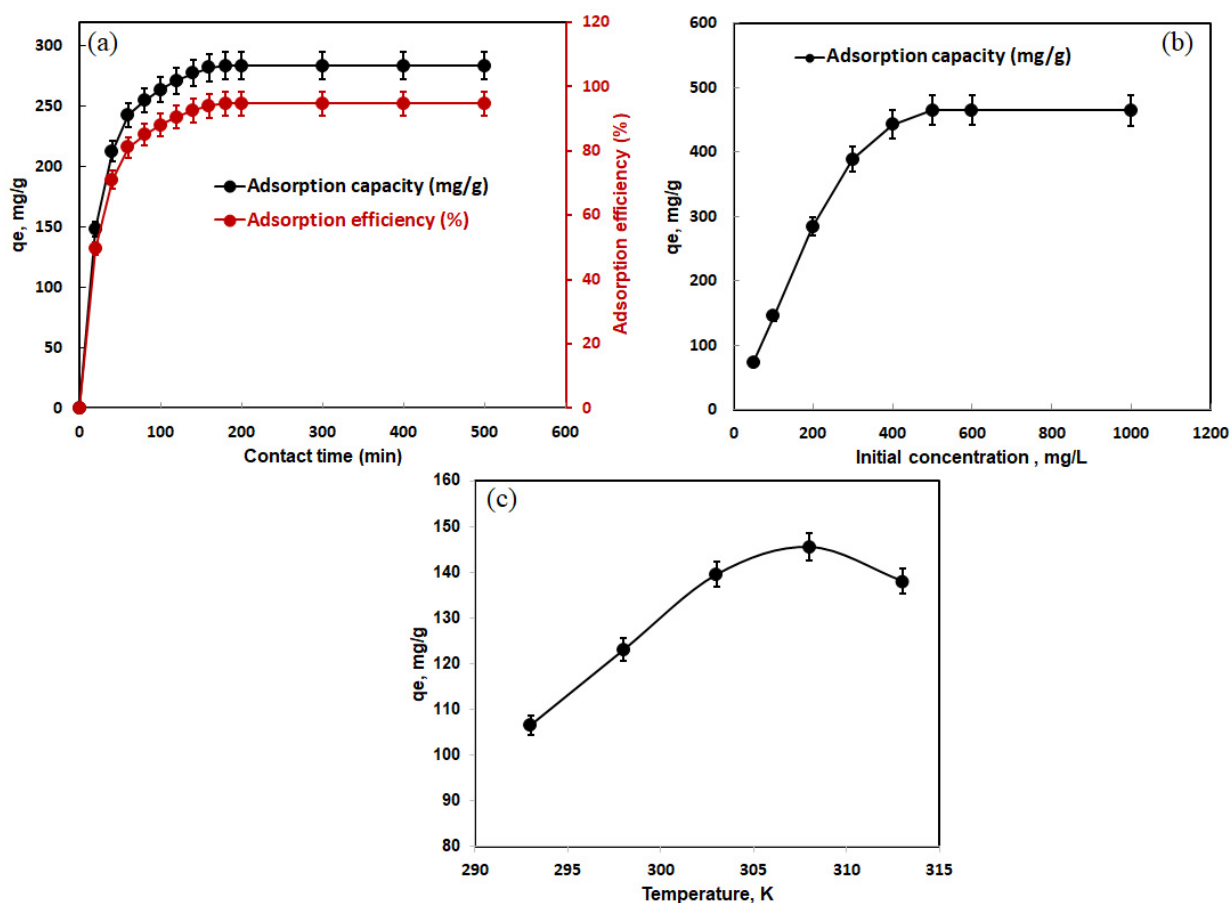


Figure 5. (a) Uptake capacity with respect to pH and (b) adsorbent dose.

The influence of the amount of TPABPOP-1 on the adsorption process was achieved in the range 0.005–0.025 g under fixed conditions ([Pb]: 100 mg/L; time: 24 h; pH: 5; and T: 298 K) as displayed in Figure 5b. The uptake efficiency increases from 88.91% to 97% with increasing mass of TPABPOP-1 adsorbent from 0.005 to 0.02 g. Beyond 0.02 g, the uptake efficiency of Pb(II) onto TPABPOP-1 adsorbent remains almost constant. This may be due to an increase in the number of the adsorption sites of Pb(II). In contrast, the adsorption capacity of TPABPOP-1 adsorbent was increased by increasing the amount of TPABPOP-1 adsorbent, owing to the fact that the uptake capacity is directly proportional to the Pb(II) ions' initial concentration and inversely proportional to the adsorbent mass as per Equation (2) [45]. Furthermore, the reduction in uptake capacity may be attributed to the aggregation of adsorbent at a high-adsorbent dose which results in a reduction in the total surface area of the TPABPOP-1. These results are in agreement with the outcomes of previous works in the literature [45,46].

The influence of contact time on the adsorption interaction was achieved in the range 20–500 min under fixed conditions ([Pb]: 100 mg/L; pH: 5; mass: 0.02 g; and T: 298 K) as presented in Figure 6a. The Pb(II) ions displayed quick adsorption, as around 50% of adsorption took place in 20 min and increased to 94.6% within 180 min. Pb(II) adsorption efficiency onto TPABPOP-1 adsorbent is nearly stable after 180 min. This may be due to the availability of active adsorption sites onto the TPABPOP-1 adsorbent in the beginning stage [47,48]. After 180 min, there was no alteration in Pb(II) ion adsorption owing to the adsorption process reaching an equilibrium state. A similar trend for the influence of equilibrium time was reported for the adsorption of Pb(II) ions on a biomass–magnetic hybrid [49] and activated carbon [50].

The impact of Pb(II) concentration on adsorption interaction was achieved in the range 50–1000 mg/L at 308 K under fixed conditions (dose: 0.02 g; pH: 5; and time: 180 min) as presented in Figure 6b. The adsorption capacity of TPABPOP-1 adsorbent toward Pb(II) ions was increased to 464.4 mg/g by enhancing the concentration of Pb(II) ions to 1000 mg/L at 308 K. This may be due to the fact that the driving force for mass transfer increases with an increase in the concentration of Pb(II) ions [51]. In addition, at the same time, the collision between Pb(II) ions and TPABPOP-1 adsorbents increased, which led to an enhancement in the uptake capacities of TPABPOP-1 toward Pb(II) ions.



**Figure 6.** (a) Uptake capacity with respect to contact time, (b) Pb(II) concentration, and (c) temperature.

The impact of temperature on the adsorption interaction was investigated at five variable temperatures (293, 298, 303, 308, and 313 K) under fixed conditions (pH: 5; mass: 0.02 g;  $C_0$ : 100 mg/L; and time: 180 min) as indicated in Figure 6c. It is evident that TPABPOP-1's adsorption capabilities toward Pb(II) ions have improved from 106.5 to 145.5 mg/g with an increase in temperature from 293 to 308 K. This is owing to the rise in temperature leading to reductions in the viscosity of the Pb(II) ion solution, which results in an increase in the rate of diffusion of Pb(II) ions through the pores of the TPABPOP-1 adsorbent [52]. Beyond 308 K, a slight drop in uptake capacity occurred, indicating the endothermic nature of adsorption. Similar observations were reported for the uptake of Pb(II) on different adsorbents such as 1,2,3-triazole-4-carboxylic acids [53] and chitosan/microbial adsorbents [54].

### 3.3. Adsorption Kinetics

Assessment of the kinetic mechanism for the uptake of Pb(II) onto the TPABPOP-1 adsorbent was achieved by analyzing the experimental kinetic data with three widely used nonlinear kinetic models, namely pseudo-first-order (PFO) [55], pseudo-second-order (PSO), and Elovich models [56]. The corresponding equations are presented in the Supplementary Material (Text S1). The fitting plots of these models and the fitting factors are indicated in Figure 7a and Table 1, respectively. The kinetic correlation coefficients ( $R^2$ ) in the PFO ( $R^2 = 0.9830$ ) model were more appropriate than those of the PSO and Elovich models. Further, the uptake quantity of Pb(II) calculated by the PFO model ( $q_{e,cal.} = 280.66$  mg/g) was close to the experimental value ( $q_{e,exp.} = 283.80$  mg/g). These outcomes suggest that the adsorption mechanism of Pb(II) onto the TPABPOP-1 adsorbent is physisorption through electrostatic interactions between Pb(II) ions and the  $NH_2$  groups on the TPABPOP-1 surface. Similar kinetic results were noticed in another previous study [57].

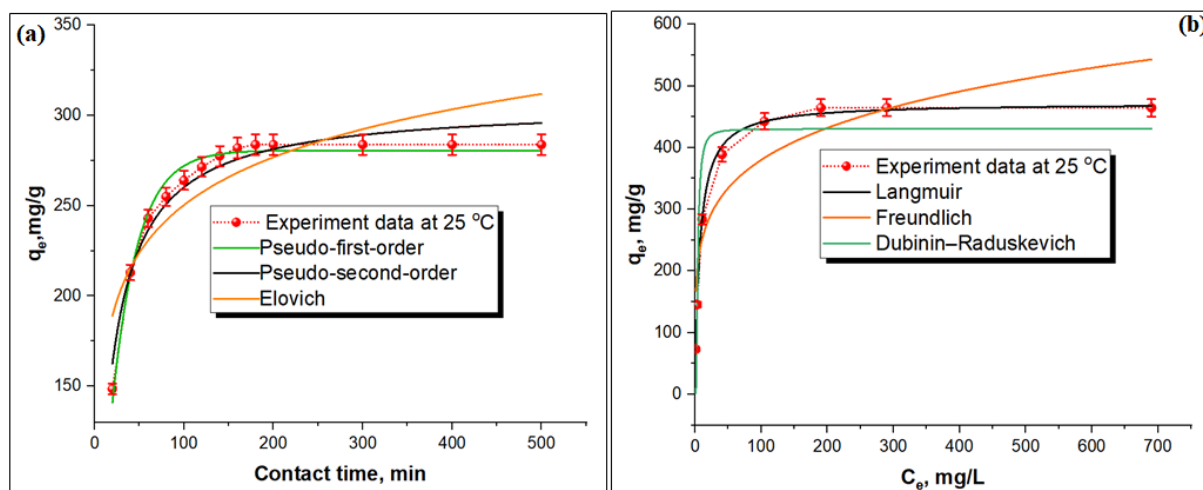


Figure 7. (a) adsorption kinetic and (b) isotherm models for uptake of Pb(II) over TPABPOP-1.

Table 1. The parameters of different kinetic models.

Model	Parameters		Value
	$C_0$ : 200 mg/L, $q_{e,exp.}$ : 283.8 mg/g		
Pseudo-first-order	$q_{e1, cal.}$ (mg/g)		280.66
	$K_1$ (1/min)		0.03
	$R^2$		0.98
Pseudo-second-order	$q_{e2, cal.}$ (mg/g)		306.2
	$K_2$ (g/mg-min)		0.00018
	$R^2$		0.96
Elovich	$\alpha$ (mg/g min)		264.89
	$B$ (mg/g)		0.03
	$R^2$		0.76

### 3.4. Adsorption Isotherms

To evaluate the adsorption mechanism of Pb(II) onto TPABPOP-1, three widely used non-linear isotherm models, namely Freundlich [58], Langmuir [59], and Dubinin–Radushkevich (D-R) [60] models were used. The corresponding equations are presented in the Supplementary Material (Text S2). The calculated parameters and fitting plots of kinetic models are presented in Table 2 and Figure 7b, respectively. According to the values of  $R^2$ , the Langmuir model ( $R^2 = 0.99763$ ) exhibited a better fit than both the Freundlich ( $R^2 = 0.80767$ ) and Dubinin–Radushkevich ( $R^2 = 0.86112$ ) models, indicating that that monolayer adsorption occurred on the surface of TPABPOP-1. At 35 °C, the maximum monolayer uptake capacity ( $q_{e,max}$ ) measured 472.20 mg/g. As presented in Table 3, the maximum quantity of Pb(II) ions adsorbed was compared with other adsorbents in order to evaluate the adsorption performance of TPABPOP-1 toward Pb(II) ions. The capacity of TPABPOP-1 is greater than most reported Pb(II) adsorbents, indicating that the TPABPOP-1 adsorbent has great potential for the elimination of Pb(II) [37,61–65]. Based on the Polanyi values in the Dubinin–Radushkevich (D–R) equation, the average adsorption potential ( $E$ ) was 0.28 kJ/mol. This value is <8.0 kJ/mol, indicating the uptake of Pb(II) on TPABPOP-1 was dominated by physical adsorption [66].

**Table 2.** The parameters of different isotherm models.

Model	Parameters	Value
	T: 308 K, $q_{e,exp.}$ : 464.4 mg/g	
Langmuir	$q_m$ , mg/g	472.20
	$K_L$ (L/mg)	0.14
	$R_L$	0.27
	$R^2$	0.99
Freundlich	$K_f$ , (mg <sup>1-n</sup> ·L <sup>n</sup> /g)	162.20
	$n$	5.41
	$R^2$	0.81
Dubinin–Radushkevich	$q_s$ , mg/g	430.39
	$K_{D-R}$ (mol <sup>2</sup> ·KJ <sup>-2</sup> )	6.27
	$E$ (kJ/mol)	0.28
	$R^2$	0.86

**Table 3.** Comparisons of various adsorbents in terms of uptake capacity.

Adsorbent	Kinetic/Isotherm Models	Temperature (K)	$q_m$ (mg/g)	Ref.
CzBPOF	PSO/Langmuir	303	318.4	[37]
Chitosan–Ninhydrin	PSO/Langmuir	298	196	[65]
UiO-66-NH <sub>2</sub>	PSO/Langmuir	298	189.69	[63]
Biochar	Intra-diffusion/Langmuir	303	92.13	[62]
Ti/Zr–DBMD	PSO/Langmuir	298	175	[64]
MnO <sub>2</sub> /PDA/Fe <sub>3</sub> O <sub>4</sub> fibers	PSO/Langmuir	318	205.074	[61]
TPABPOP-1	PFO/Langmuir	308	472.20	This study

### 3.5. Adsorption Thermodynamics

To understand the feasibility and direction of a reaction, at four different temperatures (293, 298, 303, and 308 K), batch experiments on adsorption were carried out. The enthalpy change ( $\Delta H^0$ ), entropy change ( $\Delta S^0$ ), and the Gibbs free energy ( $\Delta G^0$ ) at various temperatures were calculated with the following Equations (3) and (4):

$$\ln K_e^0 = -\frac{\Delta H^0}{RT} + \frac{\Delta S^0}{R} \quad (3)$$

$$\Delta G^0 = -RT \ln K_e^0 \quad (4)$$

$$K_e^0 = \frac{(1000 \cdot K_L \text{ molecular weight of adsorbate}) \cdot [\text{adsorbate}]^\circ}{\gamma} \quad (5)$$

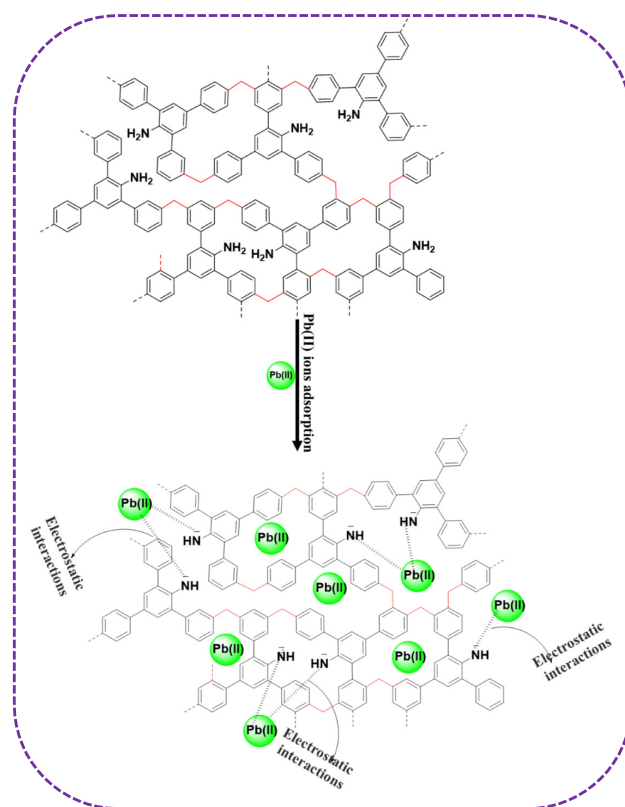
where,  $[\text{adsorbate}]^\circ$  is the standard concentration of the adsorbate (1 mol L<sup>-1</sup>) and  $\gamma$  is the coefficient of activity (dimensionless) [67].  $K_e^0$  is the thermodynamic equilibrium constant, calculated from the Langmuir model's constant of adsorption equilibrium  $K_L$  (L/mol) using Equation (5) [68–70].  $\Delta H^0$  and  $\Delta S^0$  are calculated using the Van't Hoff plot of  $\ln K_e$  vs.  $1/T$ . The values of thermodynamic factors are listed in Table 4. According to Table 4, the negative values of  $\Delta G^0$  revealed that the adsorption interaction is spontaneous in standard conditions and naturally feasible. In addition, the  $\Delta G^0$  values were reduced with the rise in temperature from 293 to 308 K, suggesting that the adsorption process is easier at high temperatures (308 K) [71]. The positive value of  $\Delta H^0$  for the uptake of Pb(II) on the TPABPOP-1 indicates the adsorption interaction was an endothermic process. Similar trends have been reported by Mu. Zheng et al. for the elimination of Pb(II) using MS-AP [72] and Xiong et al. for the elimination of Pb(II) using bio-sorbent [73]. The positive value of  $\Delta S^0$  (104.26 J/mol) means that the TPABPOP-1 and Pb(II) ions show high affinity.

**Table 4.** Thermodynamic factors for uptake of Pb(II) onto TPABPOP-1.

$\Delta H^0$ (kJ/mol)	$\Delta S^0$ (J/(mol·K))	$\Delta G^0$ (kJ/mol)			
		293 K	298 K	303 K	308 K
4.11	104.26	−26.43	−26.96	−27.49	−27.99

### 3.6. Mechanism of Adsorption

The mechanism of Pb(II) ion adsorption on TPABPOP-1 is presented in Figure 8. It was clear that the amino group is mainly responsible for Pb(II) ion adsorption as well as the uptake of Pb(II) by the porosity of TPABPOP-1 polymer. The mechanism of Pb(II) onto TPABPOP-1 was supported by FTIR spectra (Figure 3a), XPS analysis (Figure 4a), as well as pH factor. According to pH factor (Figure 3a), as the pH increases, and as the pH value rises from 2 to 5, the adsorption efficiency of TPABPOP-1 toward Pb(II) reached a maximum (97%), indicating that the amino groups of the TPABPOP-1 were deprotonated and the electrostatic interaction forces between Pb(II) and amino groups were created, which led to an improvement in the uptake capacity of TPABPOP-1. According to FTIR spectra (Figure 3a), the decrease in intensity and slight shift of NH<sub>2</sub>, N–H bending, and C–N bonds from 3423, 1622, and 1164 cm<sup>−1</sup> to 3428, 1632, and 1150 cm<sup>−1</sup>, respectively, confirmed that the Pb(II) was successfully adsorbed onto the TPABPOP-1 adsorbent. The negative charge of the amino group of TPABPOP-1 polymer can easily attract the positively charged Pb(II) by the electrostatic interaction mechanism as displayed in Figure 8. Comparing the spectra of XPS before and after the uptake of Pb(II) on TPABPOP-1, a new peak assigned to Pb 4f appeared in the spectrum of TPABPOP-1. At the same time, two peaks at 139.10 and 143.96 eV ascribed to binding energies of Pb 4f<sub>7/2</sub> and Pb 4f<sub>5/2</sub>, respectively, demonstrated that Pb(II) ions were effectively absorbed by TPABPOP-1.

**Figure 8.** Proposed mechanism of Pb(II) adsorption onto TPABPOP-1.

#### 4. Conclusions

A novel triphenylaniline-based porous organic polymer (TPABPOP-1) was synthesized by the Friedel–Crafts reaction and its applicability for the elimination of Pb(II) from water was investigated. The TPABPOP-1 was identified by different techniques, namely XPS, FTIR, SEM, TGA, BET, and  $^{13}\text{C}$  CP/MAS NMR. The surface area of TPABPOP-1 was  $1290\text{ m}^2/\text{g}$ . The uptake of Pb(II) onto TPABPOP-1 best fit to the Langmuir and PFO models. The uptake capacity of TPABPOP-1 toward Pb(II) ions was obtained as  $472.20\text{ mg/g}$  at time: 180 min; mass: 0.02 g; T: 308 K; pH: 5. FTIR and XPS techniques proved that the uptake of Pb(II) was successfully adsorbed onto TPABPOP-1. Pb(II) removal mechanisms of TPABPOP-1 may include surface adsorption and electrostatic attraction. The thermodynamic parameters exhibited that the uptake of Pb(II) onto TPABPOP-1 is spontaneous, feasible, and endothermic. These findings demonstrated the remarkable potential of synthetic TPABPOP-1 for the elimination of Pb(II) from aquatic environments.

**Supplementary Materials:** The following supporting information can be downloaded at: <https://www.mdpi.com/article/10.3390/cryst13060956/s1>. Text S1: Kinetics adsorption and Text S2: Isotherm adsorption.

**Author Contributions:** Conceptualization, S.M.; methodology, S.M. and E.H.A., software, W.A.A., B.E.-G. and Y.F.E.-A.; validation, S.M. and E.H.A.; formal analysis, H.A.A.-S. and H.E., investigation, S.M., W.A.A. and B.E.-G.; resources, S.M.; data curation, H.A.A.-S. and H.E.; writing original draft preparation, W.A.A., B.E.-G. and Y.F.E.-A.; supervision, S.M. project administration, S.M.; funding acquisition, S.M. All authors have read and agreed to the published version of the manuscript.

**Funding:** This research was funded by search and innovation agency, the Ministry of Education in Saudi Arabia, grant number [UB-27-1442], and the APC was funded by [search and innovation agency, the Ministry of Education].

**Institutional Review Board Statement:** Not applicable.

**Informed Consent Statement:** Not applicable.

**Data Availability Statement:** The data presented in this study are available on request from the corresponding authors.

**Acknowledgments:** The authors express their appreciation for the search and innovation agency, the Ministry of Education in Saudi Arabia to finance this research work through the project number (UB-27-1442).

**Conflicts of Interest:** The authors declare no conflict of interest.

#### References

1. Naushad, M.; Ahamad, T.; Al-Maswari, B.M.; Abdullah Alqadami, A.; Alshehri, S.M. Nickel ferrite bearing nitrogen-doped mesoporous carbon as efficient adsorbent for the removal of highly toxic metal ion from aqueous medium. *Chem. Eng. J.* **2017**, *330*, 1351–1360. [[CrossRef](#)]
2. Alqadami, A.A.; Naushad, M.; Allothman, Z.A.; Ghfar, A.A. Novel Metal-Organic Framework (MOF) Based Composite Material for the Sequestration of U(VI) and Th(IV) Metal Ions from Aqueous Environment. *ACS Appl. Mater. Interfaces* **2017**, *9*, 36026–36037. [[CrossRef](#)]
3. Alqadami, A.A.; Naushad, M.; Abdalla, M.A.; Ahamad, T.; Abdullah ALOthman, Z.; Alshehri, S.M.; Ghfar, A.A. Efficient removal of toxic metal ions from wastewater using a recyclable nanocomposite: A study of adsorption parameters and interaction mechanism. *J. Clean. Prod.* **2017**, *156*, 426–436. [[CrossRef](#)]
4. Ahamad, T.; Naushad, M.; Al-Maswari, B.M.; Ahmed, J.; Allothman, Z.A.; Alshehri, S.M.; Alqadami, A.A. Synthesis of a recyclable mesoporous nanocomposite for efficient removal of toxic  $\text{Hg}^{2+}$  from aqueous medium. *J. Ind. Eng. Chem.* **2017**, *53*. [[CrossRef](#)]
5. Alqadami, A.A.; Khan, M.A.; Siddiqui, M.R.; Allothman, Z.A.; Sumbul, S. A facile approach to develop industrial waste encapsulated cryogenic alginate beads to sequester toxic bivalent heavy metals. *J. King Saud. Univ.-Sci.* **2020**, *32*, 1444–1450. [[CrossRef](#)]
6. Alqadami, A.A.; Khan, M.A.; Siddiqui, M.R.; Allothman, Z.A. Development of citric anhydride anchored mesoporous MOF through post synthesis modification to sequester potentially toxic lead (II) from water. *Microporous Mesoporous Mater.* **2018**, *261*, 198–206. [[CrossRef](#)]
7. Khan, M.A.; Otero, M.; Kazi, M.; Alqadami, A.A.; Wabaidur, S.M.; Siddiqui, M.R.; Allothman, Z.A.; Sumbul, S. Unary and binary adsorption studies of lead and malachite green onto a nanomagnetic copper ferrite/drumstick pod biomass composite. *J. Hazard. Mater.* **2019**, *365*, 759–770. [[CrossRef](#)] [[PubMed](#)]

8. Alqadami, A.A.; Naushad, M.; Abdalla, M.A.; Khan, M.R.; Alothman, Z.A.; Wabaidur, S.M.; Ghfar, A.A. Determination of heavy metals in skin-whitening cosmetics using microwave digestion and inductively coupled plasma atomic emission spectrometry. *IET Nanobiotechnol.* **2017**, *11*, 597–603. [[CrossRef](#)]
9. Gibson, G.; Carlson, R.; Simpson, J.; Smeltzer, E.; Gerritson, J.; Chapra, S.; Heiskary, S.; Jones, J.; Kennedy, R. *Nutrient Criteria Technical Guidance Manual Lake and Reservoirs*; Office of Water, Office of Science and Technology: Washington, DC, USA, 2000.
10. Manechakr, P.; Karnjanakom, S. Facile utilization of magnetic  $\text{MnO}_2@Fe_3O_4$ @sulfonated carbon sphere for selective removal of hazardous Pb(II) ion with an excellent capacity: Adsorption behavior/isotherm/kinetic/thermodynamic studies. *J. Environ. Chem. Eng.* **2021**, *9*, 106191. [[CrossRef](#)]
11. Oladoye, P.O. Natural, low-cost adsorbents for toxic Pb(II) ion sequestration from (waste)water: A state-of-the-art review. *Chemosphere* **2022**, *287*, 132130. [[CrossRef](#)]
12. Machida, M.; Aikawa, M.; Tatsumoto, H. Prediction of simultaneous adsorption of Cu(II) and Pb(II) onto activated carbon by conventional Langmuir type equations. *J. Hazard. Mater.* **2005**, *120*, 271–275. [[CrossRef](#)]
13. Hong, Y.-S. Kinetic re-evaluation on “Comparative adsorption of Pb(II), Cu(II) and Cd(II) on chitosan saturated montmorillonite: Kinetic, thermodynamic and equilibrium studies”. *Appl. Clay Sci.* **2019**, *175*, 190–192. [[CrossRef](#)]
14. Kataria, N.; Garg, V.K. Optimization of Pb (II) and Cd (II) adsorption onto ZnO nanoflowers using central composite design: Isotherms and kinetics modelling. *J. Mol. Liq.* **2018**, *271*, 228–239. [[CrossRef](#)]
15. Naushad, M.; Ahamad, T.; Al-Sheetan, K.M. Development of a polymeric nanocomposite as a high performance adsorbent for Pb(II) removal from water medium: Equilibrium, kinetic and antimicrobial activity. *J. Hazard. Mater.* **2021**, *407*, 124816. [[CrossRef](#)] [[PubMed](#)]
16. Wang, T.; Jin, X.; Chen, Z.; Megharaj, M.; Naidu, R. Simultaneous removal of Pb(II) and Cr(III) by magnetite nanoparticles using various synthesis conditions. *J. Ind. Eng. Chem.* **2014**, *20*, 3543–3549. [[CrossRef](#)]
17. Naushad, M.; Alothman, Z.A.; Inamuddin; Javadian, H. Removal of Pb(II) from aqueous solution using ethylene diamine tetra acetic acid-Zr(IV) iodate composite cation exchanger: Kinetics, isotherms and thermodynamic studies. *J. Ind. Eng. Chem.* **2015**, *25*, 35–41. [[CrossRef](#)]
18. Waly, S.M.; El-Wakil, A.M.; El-Maaty, W.M.A.; Awad, F.S. Efficient removal of Pb(II) and Hg(II) ions from aqueous solution by amine and thiol modified activated carbon. *J. Saudi Chem. Soc.* **2021**, *25*, 101296. [[CrossRef](#)]
19. Ahamad, T.; Naushad, M.; Alshehri, S.M. Fabrication of magnetic polymeric resin for the removal of toxic metals from aqueous medium: Kinetics and adsorption mechanisms. *J. Water Process. Eng.* **2020**, *36*, 101284. [[CrossRef](#)]
20. Ariga, K.; Ishihara, S.; Abe, H.; Li, M.; Hill, J.P. Materials nanoarchitectonics for environmental remediation and sensing. *J. Mater. Chem.* **2012**, *22*, 2369–2377. [[CrossRef](#)]
21. Urban, J.; Svec, F.; Fréchet, J.M.J. Hypercrosslinking: New approach to porous polymer monolithic capillary columns with large surface area for the highly efficient separation of small molecules. *J. Chromatogr. A* **2010**, *1217*, 8212–8221. [[CrossRef](#)]
22. Hou, S.; Razaque, S.; Tan, B. Effects of synthesis methodology on microporous organic hyper-cross-linked polymers with respect to structural porosity, gas uptake performance and fluorescence properties. *Polym. Chem.* **2019**, *10*, 1299–1311. [[CrossRef](#)]
23. Tsyurupa, M.P.; Davankov, V.A. Porous structure of hypercrosslinked polystyrene: State-of-the-art mini-review. *React. Funct. Polym.* **2006**, *66*, 768–779. [[CrossRef](#)]
24. Waheed, A.; Baig, N.; Ullah, N.; Falath, W. Removal of hazardous dyes, toxic metal ions and organic pollutants from wastewater by using porous hyper-cross-linked polymeric materials: A review of recent advances. *J. Environ. Manage* **2021**, *287*, 112360. [[CrossRef](#)] [[PubMed](#)]
25. Hou, S.; Wang, S.; Long, X.; Tan, B. Knitting polycyclic aromatic hydrocarbon-based microporous organic polymers for efficient  $\text{CO}_2$  capture. *RSC Adv.* **2018**, *8*, 10347–10354. [[CrossRef](#)] [[PubMed](#)]
26. James, A.M.; Harding, S.; Robshaw, T.; Bramall, N.; Ogden, M.D.; Dawson, R. Selective Environmental Remediation of Strontium and Cesium Using Sulfonated Hyper-Cross-Linked Polymers (SHCPs). *ACS Appl. Mater. Interfaces* **2019**, *11*, 22464–22473. [[CrossRef](#)] [[PubMed](#)]
27. Robshaw, T.J.; James, A.M.; Hammond, D.B.; Reynolds, J.; Dawson, R.; Ogden, M.D. Calcium-loaded hydrophilic hypercrosslinked polymers for extremely high defluoridation capacity via multiple uptake mechanisms. *J. Mater. Chem. A* **2020**, *8*, 7130–7144. [[CrossRef](#)]
28. Abadast, F.; Mouradzadegan, A.; Ganjali, M.R. Rational design, fabrication and characterization of a thiol-rich 3D-porous hypercrosslink polymer as a new engineered  $\text{Hg}^{2+}$  sorbent: Enhanced selectivity and uptake. *New. J. Chem.* **2017**, *41*, 5458–5466. [[CrossRef](#)]
29. El Hefnawy, M.; Shaaban, A.F.; ElKhawaga, H.A. Effective removal of Pb(II), Cd(II) and Zn(II) from aqueous solution by a novel hyper cross-linked nanometer-sized chelating resin. *J. Environ. Chem. Eng.* **2020**, *8*, 103788. [[CrossRef](#)]
30. Algethami, J.S.; Alqadami, A.A.; Melhi, S.; Alhamami, M.A.M.; Fallatah, A.M.; Rizk, M.A. Sulfhydryl Functionalized Magnetic Chitosan as an Efficient Adsorbent for High-Performance Removal of Cd(II) from Water: Adsorption Isotherms, Kinetic, and Reusability Studies. *Adsorpt. Sci. Technol.* **2022**, *2022*, 2248249. [[CrossRef](#)]
31. Al Lafi, A.G.; Hay, J.N. 2D-COS-FTIR analysis of high molecular weight poly (N-vinyl carbazole) undergoing phase separation on purification and thermal annealing. *J. Mol. Struct.* **2019**, *1175*, 152–162. [[CrossRef](#)]
32. Ranganathan, N.; Mahalingam, G. 2,4,6-Triphenylaniline nanoemulsion formulation, optimization, and its application in type 2 diabetes mellitus. *J. Cell. Physiol.* **2019**, *234*, 22505–22516. [[CrossRef](#)] [[PubMed](#)]

33. Wu, R.; Zhao, K.; Lv, W.; Xu, J.; Hu, J.; Liu, H.; Wang, H. Solid-phase synthesis of bi-functionalized porous organic polymer for simultaneous removal of Hg(II) and Pb(II). *Microporous Mesoporous Mater.* **2021**, *316*, 110942. [[CrossRef](#)]
34. Çiçek, B.; Çağlı, M.; Tülek, R.; Teke, A. Synthesis and optical characterization of bipod carbazole derivatives. *Heterocycl. Commun.* **2020**, *26*, 148–156. [[CrossRef](#)]
35. Melhi, S.; Algamdi, M.; Alqadami, A.A.; Khan, M.A.; Alosaimi, E.H. Fabrication of magnetically recyclable nanocomposite as an effective adsorbent for the removal of malachite green from water. *Chem. Eng. Res. Des.* **2022**, *177*, 843–854. [[CrossRef](#)]
36. Sabri, M.A.; Al-Sayah, M.H.; Sen, S.; Ibrahim, T.H.; El-Kadri, O.M. Fluorescent aminal linked porous organic polymer for reversible iodine capture and sensing. *Sci. Rep.* **2020**, *10*, 15943. [[CrossRef](#)] [[PubMed](#)]
37. Melhi, S. Novel carbazole-based porous organic frameworks (CzBPOF) for efficient removal of toxic Pb(II) from water: Synthesis, characterization, and adsorption studies. *Environ. Technol. Innov.* **2022**, *25*, 102172. [[CrossRef](#)]
38. Shit, S.C.; Khilari, S.; Mondal, I.; Pradhan, D.; Mondal, J. The Design of a New Cobalt Sulfide Nanoparticle Implanted Porous Organic Polymer Nanohybrid as a Smart and Durable Water-Splitting Photoelectrocatalyst. *Chem.–A Eur. J.* **2017**, *23*, 14827–14838. [[CrossRef](#)]
39. Chen, T.; Li, W.-Q.; Hu, W.-B.; Hu, W.-J.; Liu, Y.A.; Yang, H.; Wen, K. Direct synthesis of covalent triazine-based frameworks (CTFs) through aromatic nucleophilic substitution reactions. *RSC Adv.* **2019**, *9*, 18008–18012. [[CrossRef](#)]
40. Zhang, B.-L.; Qiu, W.; Wang, P.-P.; Liu, Y.-L.; Zou, J.; Wang, L.; Ma, J. Mechanism study about the adsorption of Pb(II) and Cd(II) with iron-trimesic metal-organic frameworks. *Chem. Eng. J.* **2020**, *385*, 123507. [[CrossRef](#)]
41. Usman, M.; Ahmed, A.; Ji, Z.; Yu, B.; Shen, Y.; Cong, H. Environmentally friendly fabrication of new  $\beta$ -Cyclodextrin/ZrO<sub>2</sub> nanocomposite for simultaneous removal of Pb(II) and BPA from water. *Sci. Total. Environ.* **2021**, *784*, 147207. [[CrossRef](#)]
42. Xu, G.-R.; An, Z.-H.; Xu, K.; Liu, Q.; Das, R.; Zhao, H.-L. Metal organic framework (MOF)-based micro/nanoscaled materials for heavy metal ions removal: The cutting-edge study on designs, synthesis, and applications. *Coord. Chem. Rev.* **2021**, *427*, 213554. [[CrossRef](#)]
43. Bhaumik, M.; Maity, A.; Brink, H.G. Zero valent nickel nanoparticles decorated polyaniline nanotubes for the efficient removal of Pb(II) from aqueous solution: Synthesis, characterization and mechanism investigation. *Chem. Eng. J.* **2021**, *417*, 127910. [[CrossRef](#)]
44. Culita, D.C.; Simonescu, C.M.; Patescu, R.-E.; Dragne, M.; Stanica, N.; Oprea, O. o-Vanillin functionalized mesoporous silica-coated magnetite nanoparticles for efficient removal of Pb(II) from water. *J. Solid State Chem.* **2016**, *238*, 311–320. [[CrossRef](#)]
45. Aldawsari, A.M.; Alshohaimi, I.H.; Al-Kahtani, A.A.; Alqadami, A.A.; Ali Abdalla, Z.E.; Saleh, E.A.M. Adsorptive performance of aminoterephthalic acid modified oxidized activated carbon for malachite green dye: Mechanism, kinetic and thermodynamic studies. *Sep. Sci. Technol.* **2021**, *56*, 835–846. [[CrossRef](#)]
46. Geng, Y.; Zhang, J.; Zhou, J.; Lei, J. Study on adsorption of methylene blue by a novel composite material of TiO<sub>2</sub> and alum sludge. *RSC Adv.* **2018**, *8*, 32799–32807. [[CrossRef](#)]
47. Alhumaimess, M.S.; Alshohaimi, I.H.; Alqadami, A.A.; Khan, M.A.; Kamel, M.M.; Aldosari, O.; Siddiqui, M.R.; Hamedelniei, A.E. Recyclable glutaraldehyde cross-linked polymeric tannin to sequester hexavalent uranium from aqueous solution. *J. Mol. Liq.* **2019**, *281*, 29–38. [[CrossRef](#)]
48. Naushad, M.; Alqadami, A.A.; Ahamad, T. Removal of Cd(II) ion from aqueous environment using triaminotriethoxysilane grafted oxidized activated carbon synthesized via activation and subsequent silanization. *Environ. Technol. Innov.* **2020**, *18*, 100686. [[CrossRef](#)]
49. Mohubedu, R.P.; Diagboya, P.N.E.; Abasi, C.Y.; Dikio, E.D.; Mtunzi, F. Magnetic valorization of biomass and biochar of a typical plant nuisance for toxic metals contaminated water treatment. *J. Clean. Prod.* **2019**, *209*, 1016–1024. [[CrossRef](#)]
50. Cechinel, M.A.P.; Ulson de Souza, S.M.A.G.; Ulson de Souza, A.A. Study of lead (II) adsorption onto activated carbon originating from cow bone. *J. Clean. Prod.* **2014**, *65*, 342–349. [[CrossRef](#)]
51. Tharaneedhar, V.; Kumar, P.S.; Saravanan, A.; Ravikumar, C.; Jaikumar, V. Prediction and interpretation of adsorption parameters for the sequestration of methylene blue dye from aqueous solution using microwave assisted corncob activated carbon. *Sustain. Mater. Technol.* **2017**, *11*, 1–11. [[CrossRef](#)]
52. Jiao, X.; Zhang, L.; Qiu, Y.; Yuan, Y. A new adsorbent of Pb(ii) ions from aqueous solution synthesized by mechanochemical preparation of sulfonated expanded graphite. *RSC Adv.* **2017**, *7*, 38350–38359. [[CrossRef](#)]
53. Yuan, S.; Zhang, J.; Yang, Z.; Tang, S.; Liang, B.; Pehkonen, S.O. Click functionalization of poly(glycidyl methacrylate) microspheres with triazole-4-carboxylic acid for the effective adsorption of Pb(ii) ions. *New. J. Chem.* **2017**, *41*, 6475–6488. [[CrossRef](#)]
54. Khanniri, E.; Yousefi, M.; Mortazavian, A.M.; Khorshidian, N.; Sohrabvandi, S.; Arab, M.; Koushki, M.R. Effective removal of lead (II) using chitosan and microbial adsorbents: Response surface methodology (RSM). *Int. J. Biol. Macromol.* **2021**, *178*, 53–62. [[CrossRef](#)] [[PubMed](#)]
55. Lagergren, S. About the theory of so-called adsorption of soluble substances. *Handlingar* **1898**, *24*, 1–39.
56. Chien, S.H.; Clayton, W.R. The catalytic oxidation of carbon monoxide on manganese dioxide. *Sci. Soc. Am. J.* **1980**, *44*, 265–268. [[CrossRef](#)]
57. Yang, W.; Cheng, M.; Han, Y.; Luo, X.; Li, C.; Tang, W.; Yue, T.; Li, Z. Heavy metal ions' poisoning behavior-inspired etched UiO-66/CTS aerogel for Pb(II) and Cd(II) removal from aqueous and apple juice. *J. Hazard. Mater.* **2021**, *401*, 123318. [[CrossRef](#)]
58. Freundlich, H. Über die Adsorption in Lösungen. *Z. Für Phys. Chem.* **1907**, *57U*, 385. [[CrossRef](#)]

59. Wallis, A.; Dollard, M.F. Local and global factors in work stress—The Australian dairy farming exemplar. *Scand. J. Work Environ. Health Suppl.* **2008**, *66*, 66–74.
60. Dubinin, M.M.; Radushkevich, L.V. Equation of the characteristic curve of activated charcoal. *Proc. Acad. Sci. USSR Phys. Chem. Sect.* **1947**, *1*, 857.
61. Shi, S.; Xu, C.; Dong, Q.; Wang, Y.; Zhu, S.; Zhang, X.; Tak Chow, Y.; Wang, X.; Zhu, L.; Zhang, G.; et al. High saturation magnetization MnO<sub>2</sub>/PDA/Fe<sub>3</sub>O<sub>4</sub> fibers for efficient Pb(II) adsorption and rapid magnetic separation. *Appl. Surf. Sci.* **2021**, *541*, 148379. [[CrossRef](#)]
62. Dinh, V.-P.; Nguyen, D.-K.; Luu, T.-T.; Nguyen, Q.-H.; Tuyen, L.A.; Phong, D.D.; Kiet, H.A.T.; Ho, T.-H.; Nguyen, T.T.P.; Xuan, T.D.; et al. Adsorption of Pb(II) from aqueous solution by pomelo fruit peel-derived biochar. *Mater. Chem. Phys.* **2022**, *285*, 126105. [[CrossRef](#)]
63. Wang, H.; Wang, S.; Wang, S.; Tang, J.; Chen, Y.; Zhang, L. Adenosine-functionalized UiO-66-NH<sub>2</sub> to efficiently remove Pb(II) and Cr(VI) from aqueous solution: Thermodynamics, kinetics and isothermal adsorption. *J. Hazard. Mater.* **2022**, *425*, 127771. [[CrossRef](#)]
64. Chen, Y.; Tang, J.; Wang, S.; Zhang, L.; Sun, W. Bimetallic coordination polymer for highly selective removal of Pb(II): Activation energy, isosteric heat of adsorption and adsorption mechanism. *Chem. Eng. J.* **2021**, *425*, 131474. [[CrossRef](#)]
65. Chen, Y.; Tang, J.; Wang, S.; Zhang, L. Ninhydrin-functionalized chitosan for selective removal of Pb(II) ions: Characterization and adsorption performance. *Int. J. Biol. Macromol.* **2021**, *177*, 29–39. [[CrossRef](#)]
66. Bai, C.; Wang, L.; Zhu, Z. Adsorption of Cr(III) and Pb(II) by graphene oxide/alginate hydrogel membrane: Characterization, adsorption kinetics, isotherm and thermodynamics studies. *Int. J. Biol. Macromol.* **2020**, *147*, 898–910. [[CrossRef](#)]
67. Raymond, C.; Thoman, J.W. *Physical Chemistry for the Chemical Sciences*; University Science Books: Sausalito, CA, USA, 2014.
68. Lima, E.C.; Hosseini-Bandegharaei, A.; Moreno-Piraján, J.C.; Anastopoulos, I. A critical review of the estimation of the thermodynamic parameters on adsorption equilibria. Wrong use of equilibrium constant in the Van't Hoof equation for calculation of thermodynamic parameters of adsorption. *J. Mol. Liq.* **2018**, *273*, 425–434. [[CrossRef](#)]
69. Lima, E.C.; Hosseini-Bandegharaei, A.; Anastopoulos, I. Response to “Some remarks on a critical review of the estimation of the thermodynamic parameters on adsorption equilibria. Wrong use of equilibrium constant in the van't Hoff equation for calculation of thermodynamic parameters of adsorption—Journal of Molecular Liquids 273 (2019) 425–434.”. *J. Mol. Liq.* **2019**, *280*, 298–300. [[CrossRef](#)]
70. Azizian, S.; Eris, S.; Wilson, L.D. Re-evaluation of the century-old Langmuir isotherm for modeling adsorption phenomena in solution. *Chem. Phys.* **2018**, *513*, 99–104. [[CrossRef](#)]
71. Yu, H.; Shao, P.; Fang, L.; Pei, J.; Ding, L.; Pavlostathis, S.G.; Luo, X. Palladium ion-imprinted polymers with PHEMA polymer brushes: Role of grafting polymerization degree in anti-interference. *Chem. Eng. J.* **2019**, *359*, 176–185. [[CrossRef](#)]
72. Zheng, L.; Yang, Y.; Zhang, Y.; Zhu, T.; Wang, X. Functionalization of SBA-15 mesoporous silica with bis-schiff base for the selective removal of Pb(II) from water. *J. Solid State Chem.* **2021**, *301*, 122320. [[CrossRef](#)]
73. Xiong, C.; Xue, C.; Huang, L.; Hu, P.; Fan, P.; Wang, S.; Zhou, X.; Yang, Z.; Wang, Y.; Ji, H. Enhanced selective removal of Pb(II) by modification low-cost bio-sorbent: Experiment and theoretical calculations. *J. Clean. Prod.* **2021**, *316*, 128372. [[CrossRef](#)]

**Disclaimer/Publisher's Note:** The statements, opinions and data contained in all publications are solely those of the individual author(s) and contributor(s) and not of MDPI and/or the editor(s). MDPI and/or the editor(s) disclaim responsibility for any injury to people or property resulting from any ideas, methods, instructions or products referred to in the content.